

Air Force Institute of Technology

AFIT Scholar

Faculty Publications

11-15-2017

Power-law Schell-model Sources

Milo W. Hyde IV

Air Force Institute of Technology

Follow this and additional works at: <https://scholar.afit.edu/facpub>



Part of the [Optics Commons](#)

Recommended Citation

Hyde, M. W. (2017). Power-law Schell-model sources. *Optics Communications*, 403, 312–316.
<https://doi.org/10.1016/j.optcom.2017.07.057>

This Article is brought to you for free and open access by AFIT Scholar. It has been accepted for inclusion in Faculty Publications by an authorized administrator of AFIT Scholar. For more information, please contact AFIT.ENWL.Repository@us.af.mil.



Power-law Schell-model sources

Milo W. Hyde IV¹

Department of Electrical and Computer Engineering, Air Force Institute of Technology, Dayton, OH 45433, USA



ARTICLE INFO

Keywords:
Coherence
Random sources
Statistical optics

ABSTRACT

A new type of Schell-model source is developed that has a spectral degree of coherence, or spatial power spectrum, which is described by a power-law function. These power-law sources generally produce cusped, or peaked far-zone spectral density patterns making them potentially useful in directed energy applications. The spectral degrees of coherence, spatial power spectra, and spatial coherence radii for power-law sources are derived and discussed. Two power-law sources are then synthesized in the laboratory using a liquid crystal spatial light modulator. The experimental spectral densities are compared to the corresponding theoretical predictions to serve as a proof of concept.

Published by Elsevier B.V. This is an open access article under the CC BY license (<http://creativecommons.org/licenses/by/4.0/>).

1. Introduction

Much work has been performed designing partially coherent sources which behave in novel and exploitable ways. The literature is replete with sources that produce ring-shaped, frame-like, and cusped intensity (in the space-frequency domain, spectral density) patterns [1–3]. In addition, partially coherent sources which “self steer,” “self split,” and “rotate” have also been developed [4–6]. The interested reader is referred to [7–11] for excellent books and reviews on the subject.

In this paper, a new class of partially coherent source is introduced and synthesized. These, so called power-law sources, possess spatial coherence functions which have, or produce spectral densities with, $\rho^{-\alpha}$ dependence. These sources, like the sources in [3], can produce cusped spectral densities making them potentially useful in laser manufacturing, free-space optical communications, directed energy, et cetera. In addition, since many natural processes are well described by power-law formulas, these sources could potentially serve as simple models of light’s interaction with power-law phenomena.

In the next section, power-law sources are analytically developed. Expressions for the spectral degrees of coherence μ , spatial power spectra, and spatial coherence radii δ are derived and discussed. In addition, the asymptotic behaviors of μ and δ as the power $\alpha \rightarrow \infty$ are also determined. Lastly, in Section 3, power-law sources are physically realized in the laboratory. The experimental far-zone spectral densities S are compared to the theoretical S (also derived in Section 2) to validate the analysis.

2. Theory

From the work of Gori and Santarsiero [12], the sufficient condition for a genuine cross-spectral density function W is

$$W(\rho_1, \rho_2) = \iint_{-\infty}^{\infty} p(\mathbf{v}) H(\rho_1, \mathbf{v}) H^*(\rho_2, \mathbf{v}) d^2v, \quad (1)$$

where $\rho = \hat{x}x + \hat{y}y$, H is an arbitrary kernel, and p is a non-negative function. The dependence of the functions in (1) on radian frequency ω has been omitted for brevity. Letting $H(\rho, \mathbf{v}) = \tau(\rho) \exp(-j2\pi\rho \cdot \mathbf{v})$, where τ is a complex function, simplifies (1) to

$$W(\rho_1, \rho_2) = \tau(\rho_1) \tau^*(\rho_2) \iint_{-\infty}^{\infty} p(\mathbf{v}) \exp[-j2\pi(\rho_1 - \rho_2) \cdot \mathbf{v}] d^2v. \quad (2)$$

If the Fourier transform of p exists, then (2) describes a Schell-model source [7,8,13] with μ equal to

$$\mu(\Delta\rho) = \iint_{-\infty}^{\infty} p(\mathbf{v}) \exp(-j2\pi\Delta\rho \cdot \mathbf{v}) d^2v, \quad (3)$$

where $\Delta\rho = \rho_1 - \rho_2$. Eq. (3) is the spatial-domain form of the Wiener–Khinchin theorem [7,13]; thus, p is the spatial power spectrum of the random source. Assuming that μ (and subsequently p) is rotationally invariant transforms (3) into a Fourier–Bessel integral, viz.,

$$\begin{aligned} \mu(\rho) &= 2\pi \int_0^{\infty} v p(v) J_0(2\pi v \rho) dv \\ p(v) &= 2\pi \int_0^{\infty} \rho \mu(\rho) J_0(2\pi v \rho) d\rho, \end{aligned} \quad (4)$$

where J_0 is a zeroth-order Bessel function of the first kind and $\rho = |\Delta\rho|$ has been introduced for notational convenience.

¹ E-mail address: milo.hyde@afit.edu.

¹ The views expressed in this paper are those of the authors and do not reflect the official policy or position of the U.S. Air Force, the Department of Defense, or the U.S. Government.

2.1. Power-law μ sources

Inspired by the von Kármán atmospheric turbulence power spectrum [14], let μ be

$$\mu(\rho) = \frac{\rho_c^{2\alpha}}{(\rho^2 + \rho_c^2)^\alpha}, \tag{5}$$

where $\alpha > 1$ and $\rho_c > 0$ is related to the spatial coherence radius of the source (discussed further in Section 2.3). Substituting (5) into (4) and evaluating the integral yields

$$p(v) = \frac{2\pi\rho_c^2}{2^{\alpha-1}\Gamma(\alpha)} (2\pi\rho_c v)^{\alpha-1} K_{\alpha-1}(2\pi\rho_c v), \tag{6}$$

where Γ is the Gamma function and K is a modified Bessel function of the second kind [15].

2.2. Power-law p sources

A source with a power-law spatial power spectrum can be derived by exploiting the symmetry of the Fourier-Bessel transform in (4). Let μ be

$$\mu(\rho) = \frac{2^{2-\alpha}}{\Gamma(\alpha-1)} \left(\frac{\rho}{\rho_c}\right)^{\alpha-1} K_{\alpha-1}\left(\frac{\rho}{\rho_c}\right). \tag{7}$$

Substituting (7) into (4) and evaluating the integral produces [15,16]

$$p(v) = \frac{4\pi(\alpha-1)\rho_c^2}{[1+(2\pi\rho_c v)^2]^\alpha}. \tag{8}$$

2.3. Spatial coherence radii

The spatial coherence radii δ can be found by evaluating

$$A_c \approx \pi\delta^2 = \iint_{-\infty}^{\infty} |\mu(\rho)|^2 d^2\rho, \tag{9}$$

where A_c is the coherence area [13]. Substituting (5) into (9), evaluating the integral, and solving for δ yields

$$\delta = \frac{\rho_c}{\sqrt{2\alpha-1}}. \tag{10}$$

The value of μ at δ can be found by substituting (10) into (5) and simplifying:

$$\mu(\delta) = \left(1 - \frac{1}{2\alpha}\right)^\alpha. \tag{11}$$

For power-law p sources, evaluating (9) directly is difficult. However, one can exploit Parseval's theorem [13] and arrive at a relation for δ much more easily, viz.,

$$\delta = \sqrt{\frac{1}{\pi} \iint_{-\infty}^{\infty} |p(\mathbf{v})|^2 d^2v} = \frac{2(\alpha-1)}{\sqrt{2\alpha-1}} \rho_c. \tag{12}$$

The value of μ at δ is

$$\mu(\delta) = \frac{2^{2-\alpha}}{\Gamma(\alpha-1)} \left(2\frac{\alpha-1}{\sqrt{2\alpha-1}}\right)^{\alpha-1} K_{\alpha-1}\left(2\frac{\alpha-1}{\sqrt{2\alpha-1}}\right). \tag{13}$$

Clearly, from (10) and (12), the spatial coherence radii change with the power α . It would be preferable if δ had the same physical meaning regardless of α . This can be achieved by expressing μ and p in terms of

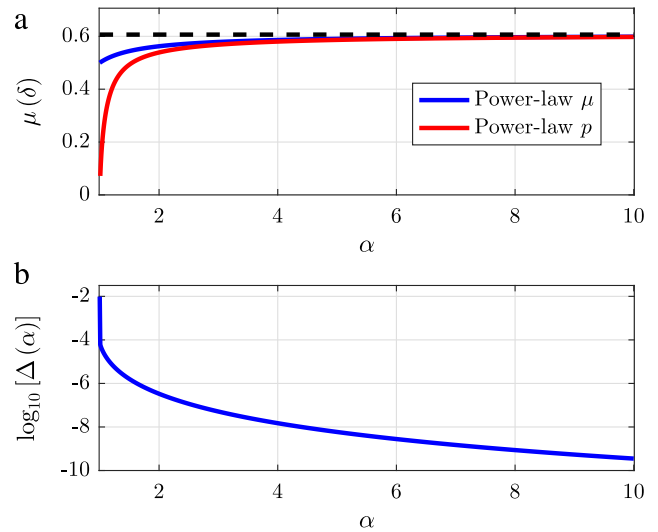


Fig. 1. (a) $\mu(\delta)$ versus α for the power-law μ and power-law p sources and (b) log of the sum of squared difference Δ versus α for the two μ given in (14).

δ instead of ρ_c :

$$\mu(\rho) = \begin{cases} \left[\frac{\delta^2(2\alpha-1)}{\rho^2 + \delta^2(2\alpha-1)} \right]^\alpha \\ \frac{2^{2-\alpha}}{\Gamma(\alpha-1)} \left(2\frac{\alpha-1}{\sqrt{2\alpha-1}}\frac{\rho}{\delta}\right)^{\alpha-1} K_{\alpha-1}\left(2\frac{\alpha-1}{\sqrt{2\alpha-1}}\frac{\rho}{\delta}\right) \end{cases} \tag{14}$$

$$p(v) = \begin{cases} \frac{2\pi(2\alpha-1)\delta^2}{2^{\alpha-1}\Gamma(\alpha)} (2\pi v\delta\sqrt{2\alpha-1})^{\alpha-1} K_{\alpha-1}(2\pi v\delta\sqrt{2\alpha-1}) \\ \frac{\pi(2\alpha-1)(\alpha-1)^{\alpha-1}\delta^2}{[(\alpha-1)^2 + \pi^2(2\alpha-1)\delta^2v^2]^\alpha} \end{cases}$$

The asymptotic behaviors of δ as $\alpha \rightarrow \infty$ are quite clear from (10) and (12), i.e., 0 and ∞ , respectively. Interestingly, the behaviors of $\mu(\delta)$ as $\alpha \rightarrow \infty$ are equal for both the power-law μ and power-law p sources—both are $\exp(-1/2) \approx 0.6065$. Fig. 1(a) shows $\mu(\delta)$ versus α for both sources. The black dashed line is the asymptotic value $\exp(-1/2)$. For $\alpha > 4$, the $\mu(\delta)$ are practically identical. As might be expected from these results, the corresponding μ (and consequently the p) given in (14) are also very similar for $\alpha > 4$. This is verified in Fig. 1(b) which shows the sum of squared difference Δ for the two μ in (14), i.e.,

$$\Delta(\alpha) = \int_0^\infty |\mu_1(\rho, \alpha) - \mu_2(\rho, \alpha)|^2 d\rho \tag{15}$$

versus α . The physical significance of this is discussed in the next section.

2.4. Propagation behavior

The behavior of a power-law Schell-model source after propagating a distance z can be found by evaluating

$$W(\rho_1, \rho_2, z) = \frac{\exp\left[\frac{jk}{2z}(\rho_1^2 - \rho_2^2)\right]}{\lambda^2 z^2} \iiint_{-\infty}^{\infty} \tau(\rho'_1) \tau^*(\rho'_2) \mu(\rho'_1 - \rho'_2) \times \exp\left[\frac{jk}{2z}(\rho_1'^2 - \rho_2'^2)\right] \times \exp\left[-\frac{jk}{z}(\rho_1 \cdot \rho'_1 - \rho_2 \cdot \rho'_2)\right] d^2\rho'_1 d^2\rho'_2, \tag{16}$$

where $k = 2\pi/\lambda$, λ is the wavelength, and μ is given in (14). Considerable progress can be made by assuming that

$$\tau(\rho) = \exp\left(-\frac{\rho^2}{4\sigma^2}\right) \tag{17}$$

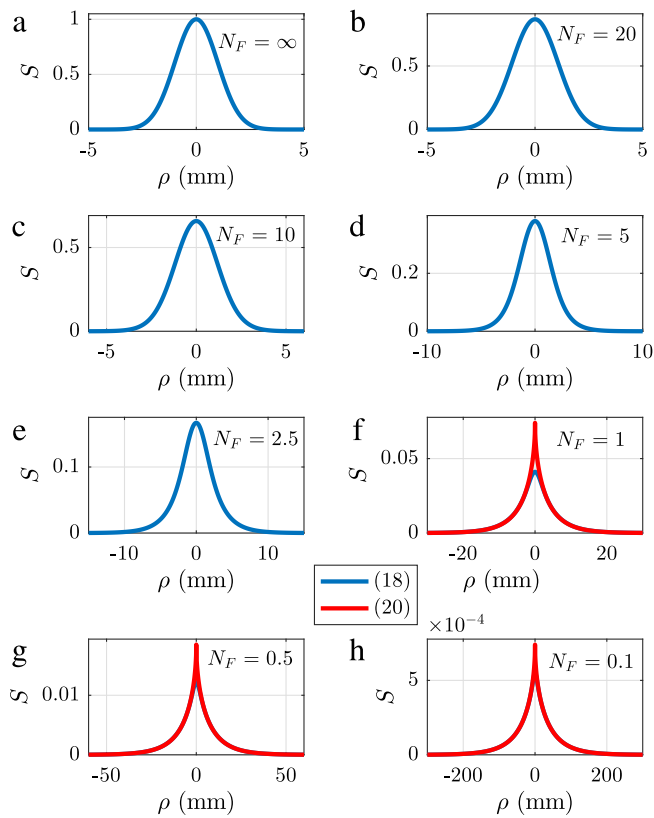


Fig. 2. Power-law μ source spectral densities S versus Fresnel number N_F —(a) $N_F = \infty$, (b) $N_F = 20$, (c) $N_F = 10$, (d) $N_F = 5$, (e) $N_F = 2.5$, (f) $N_F = 1$, (g) $N_F = 0.5$, and (h) $N_F = 0.1$. The blue traces are the S found by computing (18) numerically. The red traces in (f), (g), and (h) are the approximate far-zone S given by (20). (For interpretation of the references to color in this figure legend, the reader is referred to the web version of this article.)

and by restricting the analysis to the behavior of the spectral density S [7,8,13] versus z . Substituting (17) into (16), setting $\rho_1 = \rho_2 = \rho$, and carrying out the tedious but relatively straightforward mathematics yields

$$S(\rho, z) = W(\rho, \rho, z) = \frac{k^2 \sigma^2}{z^2} \int_0^\infty \rho' \mu(\rho') \exp\left[-\left(\frac{1}{8\sigma^2} + \frac{k^2 \sigma^2}{2z^2}\right) \rho'^2\right] \times J_0\left(\frac{k}{z} \rho \rho'\right) d\rho'. \quad (18)$$

The remaining integral (a Fourier–Bessel integral) must be computed numerically.

2.4.1. Approximate far-zone behavior

An approximate expression for the far-zone power-law source W can be found by assuming that μ is much narrower than the spectral density S . Under this condition, the source is a quasi-homogeneous source [7,8,13] and the generalized Van Cittert–Zernike theorem [13] can be used to predict the far-zone W :

$$W(\rho_1, \rho_2, z) \approx \frac{\exp\left[\frac{jk}{2z}(\rho_1^2 - \rho_2^2)\right]}{\lambda^2 z^2} \bar{S}\left(\frac{\rho_1 - \rho_2}{\lambda z}\right) p\left(\frac{\rho_1 + \rho_2}{2\lambda z}\right), \quad (19)$$

where \bar{S} is the Fourier transform of S . The far-zone spectral density can be found quite easily from (19), i.e.,

$$S(\rho, z) = \frac{1}{\lambda^2 z^2} \bar{S}(0) p\left(\frac{\rho}{\lambda z}\right). \quad (20)$$

Eq. (20) is used in Section 3 to validate the experimental results. Recall that the p given in (14) are very similar for $\alpha > 4$; thus, under this condition, both power-law sources produce similar far-zone S .

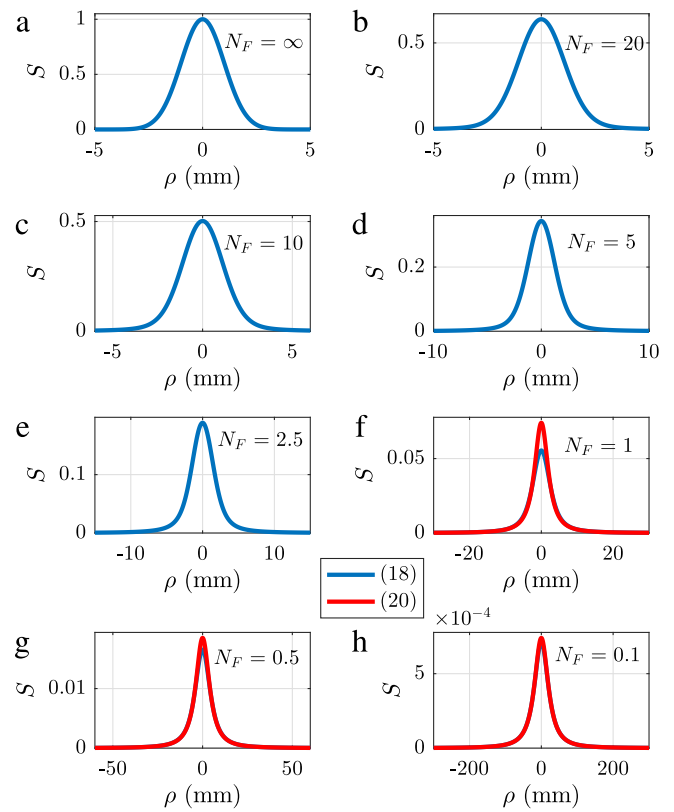


Fig. 3. Power-law ρ source spectral densities S versus Fresnel number N_F —(a) $N_F = \infty$, (b) $N_F = 20$, (c) $N_F = 10$, (d) $N_F = 5$, (e) $N_F = 2.5$, (f) $N_F = 1$, (g) $N_F = 0.5$, and (h) $N_F = 0.1$. The blue traces are the S found by computing (18) numerically. The red traces in (f), (g), and (h) are the approximate far-zone S given by (20). (For interpretation of the references to color in this figure legend, the reader is referred to the web version of this article.)

Figs. 2 and 3 show the power-law μ and power-law ρ S versus Fresnel number N_F , respectively. Here, $N_F = r^2/(\lambda z)$ [17], where $r = 2\sigma$, $\sigma = 1$ mm, and $\lambda = 1$ μ m. Additionally, $\delta = \sigma/10 = 0.1$ mm and $\alpha = 1.25$. The blue traces are the S found by computing (18) numerically; the red traces in (f), (g), and (h) are the approximate far-zone S given by (20). As expected, (20) is a very good approximation to (18) for small Fresnel numbers. Note that both sources produce cusped S in the far zone—exploitable, in practice, using a lens.

3. Experiment

3.1. Set-up

In this section, experimental results of power-law sources with μ given in (14) are presented. A schematic of the experimental set-up used to synthesize the sources is presented in Fig. 4. Light from a 632.8 nm helium–neon (HeNe) laser is expanded 20 \times before passing through a half-wave plate (HWP) and linear polarizer (LP). The HWP–LP combination serves to align the linearly polarized light exiting the laser with the control state of the spatial light modulator (SLM) – vertical in this case – and to control light power.

After passing through the HWP–LP, the light is incident on the SLM. The SLM used here is a Meadowlark Optics P512 which has a 512 \times 512 liquid crystal pixel array with a 15 μ m pitch. The light reflected from the SLM is diffracted into multiple orders. Partially coherent source instances are produced in the first diffraction order; thus, a spatial filter [composed of a 400 mm lens, an iris, and a 100 mm lens (L2)] is used to remove all orders other than desired first order.

Lastly, the random intensities are recorded by a camera located 40 cm beyond the focus of L2. The camera used here is a Lumenera

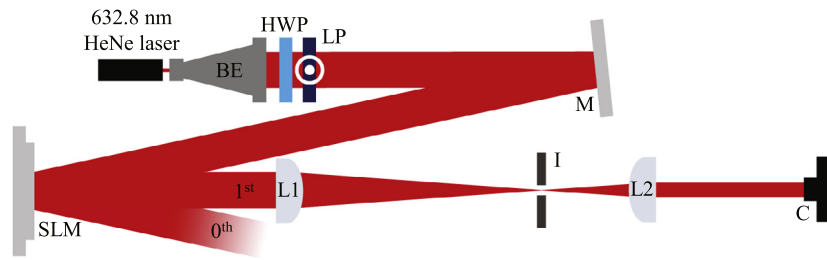


Fig. 4. Schematic of the experimental set-up. The abbreviations used in the figure are helium–neon (HeNe), beam expander (BE), half-wave plate (HWP), linear polarizer (LP), mirror (M), spatial light modulator (SLM), 400 mm lens (L1), iris (I), 100 mm lens (L2), and camera (C).

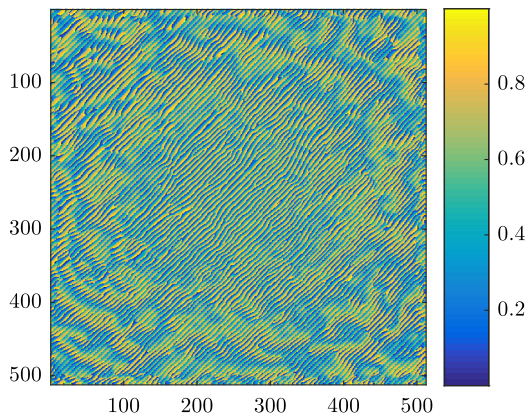


Fig. 5. Example SLM command for generating a single instance of a power-law μ source. The phase command depicted in the figure is in waves.

Lw135RM which has a 1392×1040 detector array with a $4.65 \mu\text{m}$ pitch. In addition to producing random field instances, the SLM also applies a 40 cm focus so that the intensities measured by the camera are, equivalently, the far-zone intensities.

3.2. Power-law sources & data processing

The power-law μ and power-law p sources both had Gaussian-shaped τ [see (17)], where $\sigma = 1 \text{ mm}$. The δ and α for both sources were $\delta = 0.1 \text{ mm}$ and $\alpha = 1.5$. The modified phase screen technique was used to synthesize power-law source realizations [18–20]. An example SLM command for generating a single instance of a power-law μ source is shown in Fig. 5. A detailed description of the screen (SLM command) synthesis process, including an illustration depicting the process, can be found in [20].

The experimental S were formed by averaging 5,000 measured intensities. The camera continuously collected 66 ms exposures until the sequence of 5,000 random field instances was completed. The data collect for each power-law source took approximately 225 s. The raw experimental S were then centered for ease of comparison with the theoretical S derived from (20):

$$S(\rho, z) = \frac{2\pi\sigma^2}{\lambda^2 z^2} p\left(\frac{\rho}{\lambda z}\right), \quad (21)$$

where p are given in (14).

3.3. Results

Figs. 6 and 7 shows the results for the power-law μ and power-law p sources, respectively. The layout of both figures is the same: (a) shows the theoretical spectral density S [see (21)], (b) shows the experimental S , and (c) shows the $y = 0$ slice of the theoretical and experimental normalized S . The experimental and theoretical S are in excellent agreement. Upon close inspection of Figs. 6(b) and 7(b), a cross

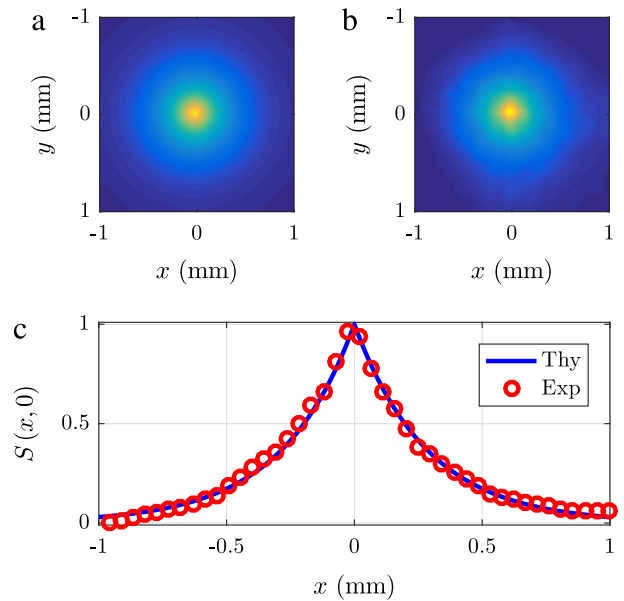


Fig. 6. Power-law μ source results—(a) theoretical S , (b) experimental S , and (c) $y = 0$ slice of theoretical and experimental normalized S .

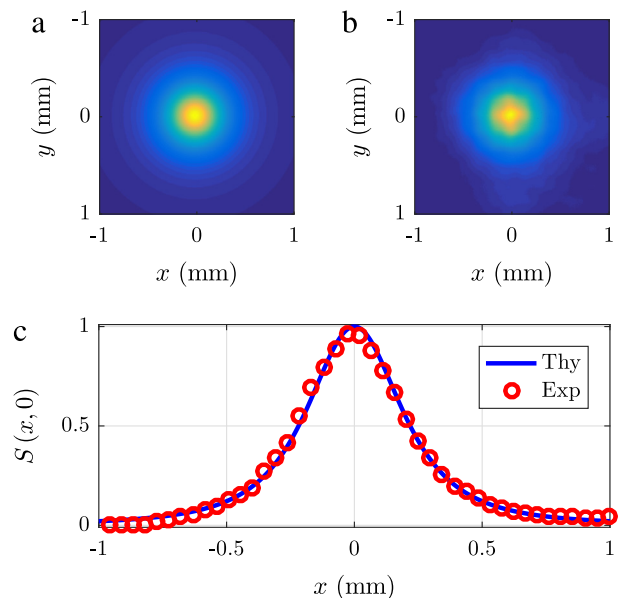


Fig. 7. Power-law p source results—(a) theoretical S , (b) experimental S , and (c) $y = 0$ slice of theoretical and experimental normalized S .

or star shape is discernable around the origin in both figures. These are very minor experimental errors and likely caused by the spatial and phase discretization of the SLM.

4. Conclusion

In this paper, Schell-model sources which possessed power-law spectral degrees of coherence μ and spatial power spectra p were developed. It was shown that these power-law sources can produce cusped, or peaked spectral densities S making them potentially useful in laser manufacturing or directed energy applications. Expressions for μ , p , and the spatial coherence radii were derived and discussed. Their asymptotic behaviors as the power $\alpha \rightarrow \infty$ were also investigated. Lastly, power-law μ and power-law p sources were physically realized in the laboratory using an SLM. The experimental S were compared to the corresponding theoretical S and found to be in excellent agreement.

References

- [1] Z. Mei, O. Korotkova, Random sources generating ring-shaped beams, *Opt. Lett.* 38 (2) (2013) 91–93. <http://dx.doi.org/10.1364/OL.38.000091>. URL <http://ol.osa.org/abstract.cfm?URI=ol-38-2-91>.
- [2] O. Korotkova, E. Shchepakina, Random sources for optical frames, *Opt. Express* 22 (9) (2014) 10622–10633. <http://dx.doi.org/10.1364/OE.22.010622>. URL <http://www.opticsexpress.org/abstract.cfm?URI=oe-22-9-10622>.
- [3] J. Li, F. Wang, O. Korotkova, Random sources for cusped beams, *Opt. Express* 24 (16) (2016) 17779–17791. <http://dx.doi.org/10.1364/OE.24.017779>. URL <http://www.opticsexpress.org/abstract.cfm?URI=oe-24-16-17779>.
- [4] Y. Chen, S.A. Ponomarenko, Y. Cai, Self-steering partially coherent beams, *Sci. Rep.* 7 (2017) 39957 URL <http://dx.doi.org/10.1038/srep39957>.
- [5] Y. Chen, J. Gu, F. Wang, Y. Cai, Self-splitting properties of a Hermite-Gaussian correlated Schell-model beam, *Phys. Rev. A* 91 (2015) 013823. <http://dx.doi.org/10.1103/PhysRevA.91.013823>. URL <http://link.aps.org/doi/10.1103/PhysRevA.91.013823>.
- [6] Z. Mei, O. Korotkova, Random sources for rotating spectral densities, *Opt. Lett.* 42 (2) (2017) 255–258. <http://dx.doi.org/10.1364/OL.42.000255>. URL <http://ol.osa.org/abstract.cfm?URI=ol-42-2-255>.
- [7] L. Mandel, E. Wolf, *Optical Coherence and Quantum Optics*, Cambridge University, New York, NY, 1995.
- [8] O. Korotkova, *Random Light Beams: Theory and Applications*, CRC, Boca Raton, FL, 2014.
- [9] G. Gbur, T. Visser, The structure of partially coherent fields, *Prog. Opt.* 55 (2010) 285–341. <http://dx.doi.org/10.1016/B978-0-444-53705-8.00005-9>. URL <http://www.sciencedirect.com/science/article/pii/B9780444537058000059>.
- [10] Y. Cai, Y. Chen, J. Yu, X. Liu, L. Liu, Generation of partially coherent beams, *Prog. Opt.* 62 (2017) 157–223. <http://dx.doi.org/10.1016/bs.po.2016.11.001>. URL <http://www.sciencedirect.com/science/article/pii/S0079663816300166>.
- [11] Y. Cai, Y. Chen, F. Wang, Generation and propagation of partially coherent beams with nonconventional correlation functions: a review, *J. Opt. Soc. Am. A* 31 (9) (2014) 2083–2096. <http://dx.doi.org/10.1364/JOSAA.31.002083>.
- [12] F. Gori, M. Santarsiero, Devising genuine spatial correlation functions, *Opt. Lett.* 32 (24) (2007) 3531–3533. <http://dx.doi.org/10.1364/OL.32.003531>. URL <http://ol.osa.org/abstract.cfm?URI=ol-32-24-3531>.
- [13] J.W. Goodman, *Statistical Optics*, second ed., Wiley, Hoboken, NJ, 2015.
- [14] L.C. Andrews, R.L. Phillips, *Laser Beam Propagation through Random Media*, second ed., SPIE Press, Bellingham, WA, 2005.
- [15] I.S. Gradshteyn, I.M. Ryzhik, *Table of Integrals, Series, and Products*, seventh ed., Academic Press, Burlington, MA, 2007, p. 678 (Chapter 6), 6.565.4.
- [16] I.S. Gradshteyn, I.M. Ryzhik, *Table of Integrals, Series, and Products*, seventh ed., Academic Press, Burlington, MA, 2007, p. 684 (Chapter 6), 6.576.7.
- [17] J.W. Goodman, *Introduction to Fourier Optics*, third ed., Roberts & Company, Englewood, CO, 2005.
- [18] M.W. Hyde IV, S. Basu, X. Xiao, D.G. Voelz, Producing any desired far-field mean irradiance pattern using a partially-coherent Schell-model source, *J. Opt.* 17 (5) (2015) 055607. <http://dx.doi.org/10.1088/2040-8978/17/5/055607>. URL <http://stacks.iop.org/2040-8986/17/i=5/a=055607>.
- [19] M.W. Hyde IV, S. Basu, D.G. Voelz, X. Xiao, Generating partially coherent Schell-model sources using a modified phase screen approach, *Opt. Eng.* 54 (12) (2015) 120501 URL <http://dx.doi.org/10.1117/1.OE.54.12.120501>.
- [20] M.W. Hyde, S. Bose-Pillai, D.G. Voelz, X. Xiao, Generation of vector partially coherent optical sources using phase-only spatial light modulators, *Phys. Rev. Appl.* 6 (2016) 064030. <http://dx.doi.org/10.1103/PhysRevApplied.6.064030>. URL <https://link.aps.org/doi/10.1103/PhysRevApplied.6.064030>.